

# Efficient framework for the simulation of translational and rotational laser speckle displacement in optical sensor assemblies

Ernst Csencsics<sup>✉,\*</sup>, Tobias Wolf, and Georg Schitter<sup>✉</sup>

Automation and Control Institute, Technische Universität Wien, Vienna, Austria

**Abstract.** The optimization and uncertainty analysis of laser-based optical sensors in the design phase is a challenging task due to the presence of stochastic laser speckle effects. We present an accurate, efficient, and versatile simulation framework for the design of optical sensor assemblies, capable of handling objective as well as subjective speckle effects. The framework integrates the stochastic nature of laser speckle with the deterministic properties of ray-tracing simulations, enabling the simulation of sensitivities to translational as well as rotational target motion and reliable performance estimation, even for more complex optical assemblies. To validate the simulation results for translation and rotation, they are compared against the experimental data of four speckle-based optical sensor assemblies as well as against analytical relations for speckle pattern motion. The accuracy of the developed framework is demonstrated by simulation errors for correlation peak shift of the speckle pattern of less than  $2 \mu\text{m}$  rms and  $2.4 \mu\text{m}$  rms for translation and rotation, respectively. For the center of gravity shift as additional simulation output for an integrated laser sensor for sensing translations in all three degrees of freedom, a simulation error of  $2.6 \mu\text{m}$  rms was obtained, which also lies well below the resolution of the designed optical sensor assemblies. © 2022 Society of Photo-Optical Instrumentation Engineers (SPIE) [DOI: [10.1117/1.OE.61.6.061410](https://doi.org/10.1117/1.OE.61.6.061410)]

**Keywords:** laser speckle; speckle simulation; triangulation sensor; displacement measurement; surface tracking; in-process measurement; design tool.

Paper 20211392SS received Nov. 27, 2021; accepted for publication Feb. 2, 2022; published online Feb. 25, 2022.

## 1 Introduction

In science and industry, there are various applications that require the accurate motion tracking of an object surface by a respective tool for enabling high precision manipulations or measurements on a moving target or product piece. They range from manufacturing<sup>1,2</sup> all the way to medicine and life sciences.<sup>3,4</sup> Robot-based, high-resolution, three-dimensional inline metrology is one of the application cases that is of highest interest for the manufacturing industry.<sup>5</sup> To enable the required measurements, these systems need to actively track the motion of the target with single-micrometer precision, compensating for vibrations of the production environment in all six degrees of freedom (DoFs).<sup>1,6</sup>

For the measurement of out-of-plane translation and rotation, there are plenty of optical principles, such as laser triangulation,<sup>7</sup> available. The number of suitable concepts for measuring in-plane translation and rotation is significantly smaller, with laser speckle measurement principles being among the most promising ones. Their advantages include contact-less measurements, high resolution, and applicability to most technical surfaces without the need for additional markers.<sup>8</sup> In the past, they have so far been mainly used for strain measurements, due to their limited measurement range caused by decorrelation.<sup>9,10</sup> Advanced concepts overcoming this drawback have been developed to make them suitable for measuring the relative<sup>11</sup> and absolute position of a target,<sup>12</sup> for compensation-based measurement systems,<sup>13</sup> as well as for measuring rotational tool speeds.<sup>14</sup> Recently, also a compensation-based laser sensor, integrating laser

\*Address all correspondence to Ernst Csencsics, [csencsics@acin.tuwien.ac.at](mailto:csencsics@acin.tuwien.ac.at)

0091-3286/2022/\$28.00 © 2022 SPIE

Csencsics, Wolf, and Schitter: Efficient framework for the simulation of translational and rotational laser . . .

triangulation and objective laser speckle (OLSP) principles, has been reported for tracking in- and out-of-plane translations of a target with single micrometer precision.<sup>15</sup>

The design and uncertainty analysis of such sensors, considering also laser speckle effects, is, however, challenging,<sup>16</sup> as there are hardly any versatile simulation tools available that can be employed to estimate the performance of nontrivial sensor geometries. Existing approaches focus mostly on the stochastic nature of speckle patterns by employing two-dimensional (2D) fast Fourier transforms to generate artificial speckle patterns,<sup>17</sup> the Fourier shift theorem to describe in-plane translation,<sup>18</sup> or provide numerical simulations of dynamic speckle sequences to analyze transients of, e.g., paint drying processes.<sup>19</sup> A more recent work on the digital simulation of speckle patterns employed a generalized Huygens principle approach for the derivation of the speckle intensity.<sup>20</sup> Another contribution considered a wave-optics approach to model the effects of dynamic speckle, focusing on various spot geometries on the target and their influence on the slope of the speckle decorrelation curve.<sup>21</sup> With the capability to handle arbitrary system geometries and to estimate sensitivity and crosstalk, we recently reported a speckle simulation tool for translations of a target.<sup>22</sup>

The contributions of this paper include (i) the development of a simulation framework for simulating laser speckle effects due to translational as well as rotational motion of a target in laser-based optical sensor assemblies, (ii) an analysis of basic OLSP geometries, and (iii) the analytic as well as experimental validation of the framework accuracy based on four optical sensor configurations. The framework is capable of handling objective as well as subjective speckle in arbitrary system geometries by integrating the stochastic nature of speckle with the deterministic properties of ray-tracing simulations. It considers the system geometry including the location, orientation and size of the laser source, the target surface, the detector (with number and size of pixels) as well as apertures, lenses, or mirrors if applicable. The simulation framework enables the calculation of several system outputs, such as sensitivity or crosstalk, for designed sensor assemblies up front, to determine the best performing configuration for a given set of system requirements. Section 2 introduces the foundations of laser speckle formation and correlation, followed by a description of the numerical simulation procedure in Sec. 3. In Sec. 4, the experimental OLSP sensor assemblies are introduced and analyzed. The accuracy of the simulation framework is validated against experimental data and analytic calculations in Sec. 5, while Sec. 6 concludes the paper.

## 2 Laser Speckle Formation and Correlation

When illuminating an optically rough surface with a coherent light beam, each illuminated point on the microstructured surface can be considered as individual scatterer, scattering the incoming light randomly in direction, amplitude, and phase.<sup>23</sup> While propagating away from the target surface, the scattered light waves are interfering with each other. This interference effect can be imaged as a spatial intensity distribution in the diffraction field (free-space geometry) and the image field of the object, resulting in a grainy pattern of bright and dark spots, termed laser speckle.<sup>24</sup> When using a focused lens system, as with a typical laser triangulation sensor, subjective laser speckle (SLSP) can be observed, with the aperture limiting the spatial interaction of the individual waves emerging from the surface.<sup>8</sup> When no imaging system is used (free-space observation) OLSP patterns are observed, with the entire illuminated area contributing to the resulting speckle pattern. The lens-less case with OLSP enables in general more compact sensor designs and additionally avoids lens aberrations.<sup>24</sup>

Figure 1 shows the configuration of an OLSP-based sensor system for measuring in-plane translation or out-of-plane rotation along or around the  $x$ - and  $y$ -axes without imaging optics. Integrating a lens as imaging optics between target and observation plane would on the other hand entail the formation of SLSP. A laser in the  $xz$ -plane is used to illuminate the optically rough target surface. It is a distance  $L_S$  away from the origin  $O$  and tilted by an angle  $\Theta$  with respect to the surface normal. The image detector is placed in the observation plane, which is parallel to the object plane (without loss of generality) and located at the distance  $L_O$ . Neglecting strain on the target surface, the displacement of the speckle pattern in  $\zeta(x)$ - and  $\eta(y)$ -direction caused by a translation or rotation of the target can be expressed as<sup>24</sup>

Csencsics, Wolf, and Schitter: Efficient framework for the simulation of translational and rotational laser...

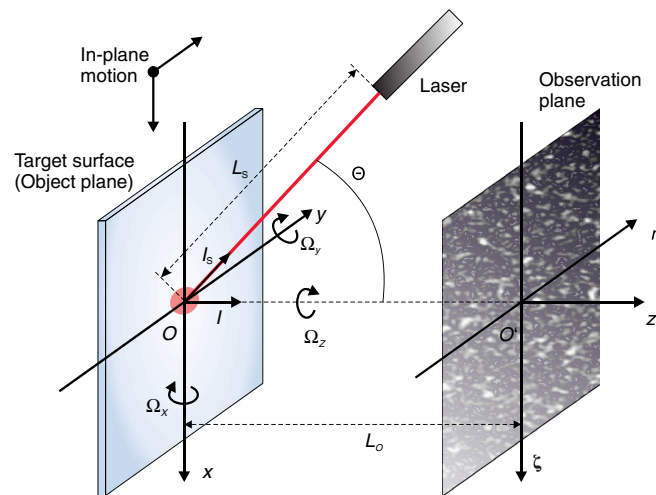


**Fig. 1** Laser speckle-based sensor configuration without imaging optics for measuring in-plane translation or out-of-plane rotation of the target. Illumination of an optically rough target surface with a coherent laser beam leads to the formation of OLSPs in the observation plane. The target translation or rotation result in a respective shift of the pattern [see Eqs. (1) and (2)].

$$A_{\zeta} = -a_x \left[ \frac{L_o}{L_s} (l_{S_x}^2 - 1) + l_x^2 - 1 \right] - a_y \left[ \frac{L_o}{L_s} l_{S_x} l_{S_y} + l_x l_y \right] - a_z \left[ \frac{L_o}{L_s} l_{S_x} l_{S_z} + l_x l_z \right] - \Omega_y [-L_o (l_{S_z} + l_z)] - \Omega_z [L_o (l_{S_y} + l_y)], \quad (1)$$

$$A_{\eta} = -a_x \left[ \frac{L_o}{L_s} l_{S_x} l_{S_y} + l_x l_y \right] - a_y \left[ \frac{L_o L_o}{L_s L_s} (l_{S_y}^2 - 1) + l_y^2 - 1 \right] - a_z \left[ \frac{L_o L_o}{L_s L_s} l_{S_y} l_{S_z} + l_y l_z \right] - \Omega_x [-L_o (l_{S_z} + l_z)] - \Omega_z [-L_o (l_{S_x} + l_x)], \quad (2)$$

where  $a_{x,y,z}$  and  $\Omega_{x,y,z}$  are the displacements of the target in the three translational and rotational DoFs, respectively. For the nominal case, of a parallel object and observation plane the simplified unit vectors  $\vec{l} = (l_x, l_y, l_z)^T = (0, 0, 1)^T$  and  $\vec{l}_S = (l_{S_x}, l_{S_y}, l_{S_z})^T = (-\sin(\Theta), 0, \cos(\Theta))^T$  given in Fig. 1 are obtained. If the two planes are not parallel, additionally small crosstalk terms need to be considered. From Eqs. (1) and (2), it is obvious that there results non-neglectable crosstalk between the translational and rotational DoFs, as five input DoFs are matched onto a single output DoF, respectively. This entails that for precise displacement sensing tasks target motion needs to be limited to a certain DoF of interest, while displacement in the other DoFs needs to be restricted as much as possible. This crosstalk aspect is again revised in Sec. 4.

For estimating the speckle pattern displacement, most commonly the 2D normalized cross-correlation function (NCC) is applied to the shifted version  $I$  and a reference image  $I_0$ .<sup>25</sup>

$$R(u, v) = \frac{\sum_{x,y} [I(x, y) - \bar{I}_{u,v}] [I_0(x - u, y - v) - \bar{I}_0]}{\sqrt{\sum_{x,y} [I(x, y) - \bar{I}_{u,v}]^2 \sum_{x,y} [I_0(x - u, y - v) - \bar{I}_0]^2}}. \quad (3)$$

It calculates the NCC coefficient in dependence for the 2-D image displacements  $u$  and  $v$ . A direct estimate for the spatial displacement is given by the position of the NCC peak value with a resolution of  $\pm 1/2$  pixel, without additional interpolation. The use of laser speckle for displacement measurement is always limited by decorrelation effects caused by three major factors: (i) changes in the microstructure due to stress or strain, (ii) the relative overlap of the correlation windows, and (iii) changes of the illumination position on the surface due to target displacement.

Csencsics, Wolf, and Schitter: Efficient framework for the simulation of translational and rotational laser...

While strain is neglected for displacement measurements and the second factor can be decreased by interpolation,<sup>26</sup> the third factor can be overcome by compensation-based sensing systems.<sup>15</sup>

### 3 Numerical Simulation of Laser Speckle

An efficient framework for the simulation of speckle displacement in optical sensor assemblies due to target translation and rotation should be capable of handling arbitrary system geometries, consider various optical elements and evaluate correlation-based shifts of the speckle pattern as well as center of gravity (CoG) shifts of a partly illumination of the detector area (triangulation sensor case) to calculate in- and out-of-plane displacements.<sup>15</sup> The simulation framework provides these properties by integrating the stochastic nature of laser speckle with the deterministic properties of the ray tracing method, making it suitable for a broad range of applications.

The basic implementation of the simulation framework and its algorithms is done in *MATLAB* (MathWorks Inc., Massachusetts) using the *Optometrika* library,<sup>27</sup> which provides ray tracing functions together with a number of optical elements. The algorithm itself consists of two parts and is illustrated in the flowchart in Fig. 2. Part 1 (left column) starts with the definition of the system geometry including the location, orientation, and size of the laser source, the target surface, the detector (with number and size of pixels), and apertures and/or lenses, if applicable. The laser spot on the target is approximated by  $N_1$  point sources, which are equally distributed within the spot diameter in  $x$  and  $y$  directions and randomly distributed within the expected surface roughness of the target material in  $z$  direction. The related intensities of the point sources are normally distributed to resemble a typical Gaussian beam intensity profile [see Fig. 3(a)]. Each of the  $N_1$  point sources (running index  $j$  in Fig. 2) is again approximated by  $N_2$  rays, which

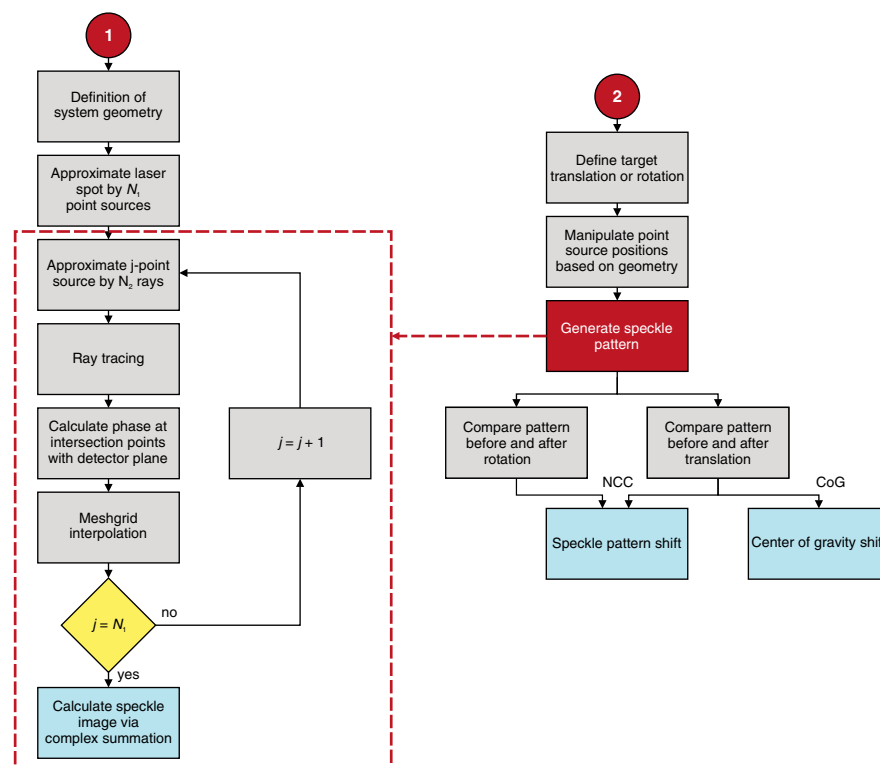


**Fig. 2** Flowchart of the simulation procedure. Part 1 shows the generation of the laser speckle image. Part 2 calculates the effects of target translations and rotations on the resulting speckle pattern and derives application specific outputs, such as the NCC peak or CoG shift.<sup>15</sup>

Csencsics, Wolf, and Schitter: Efficient framework for the simulation of translational and rotational laser...

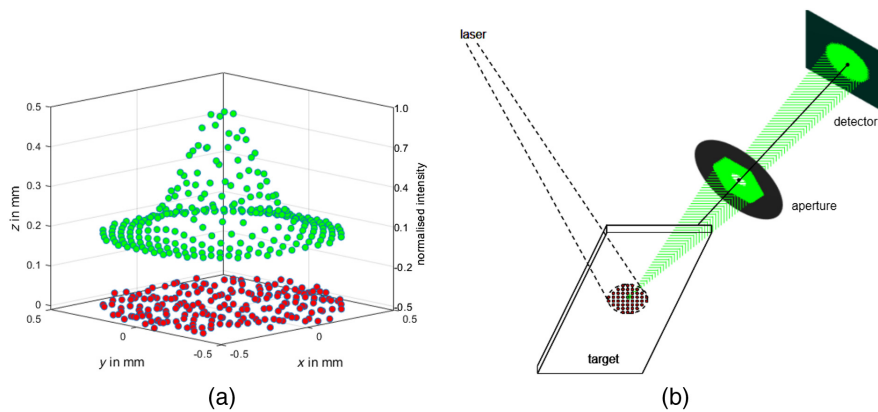


**Fig. 3** Simulation environment. (a) Approximation of the laser spot on the target with multiple point sources. The red dots are the point source locations in space, with the  $z$  values randomly distributed within the surface roughness of the target material. The green dots represent the associated Gaussian distributed intensity. (b) Ray tracing through an example system, containing an aperture and a lens. The green point source is approximated by  $N_2$  rays, which beam out under a defined solid angle and enable the calculation of a phase image on the detector for each point source.

beam out equally distributed over a preset solid angle  $\Omega$ . Using the ray tracing functions of the *Optometrika* library, each of the emerging rays is propagated toward the detector through the previously defined optical system. All rays not intersecting with the predefined detector area, as they are, for example, blocked by an aperture as shown in Fig. 3(b), are discarded for the further considerations.

With the known optical path lengths and the used laser wavelength, the phase of each ray at the intersection point with the detector can be calculated. As not all detector pixels will be hit by a ray from a specific point source, grid data interpolation with a meshgrid according to the pixel size is employed to calculate possibly missing phase values. This sequence is repeated for all point sources, until the running index  $j$  reaches the value of  $N_1$ . Using the intensity and phase image matrix of each point source on the detector, the speckle image is calculated by complex superposition of all point sources.

With the calculation of the speckle pattern according to part 1 of the algorithm, part 2 takes care of the effects of target translation and rotation and the computation of the simulation outputs (see right column in Fig. 2). A target displacement is simulated via manipulating the laser point source positions based on trigonometric relations for the defined geometry. For in-plane target translation, the absolute location of the illuminated area stays constant, while the positions of the point sources are laterally shifted according to the target translation. For out-of-plane target translation, the lateral positions of the point sources stay constant, while the absolute position of the illuminated area shifts laterally according to the laser orientation and system geometry. Small target rotations (in-plane and out-of-plane) are considered by similar point source displacements. In all cases, some of the point sources leave the illuminated spot area, which makes them essentially invalid and are replaced by new ones, added to the currently illuminated area. After adapting the point source positions and the illuminated area on the surface, a new speckle image on the detector is generated according to part 1 (see dotted box in Fig. 2). Based on the updated speckle pattern, the reference image and respective outputs depending on the application, such as the NCC correlation peak and CoG shift, can be calculated.

The formation of a representative speckle pattern requires a minimum number of point sources for approximating the laser spot on the target, which should, however, be kept as small as possible for the sake of computational efficiency. In Figs. 4(b)–4(d), the resulting intensity distribution of the speckle pattern on the detector is shown for the basic OLSP setup configuration from Fig. 1 with an additional 1 mm aperture between target surface and observation plane.<sup>15</sup> In Fig. 4(a), the phase image on the detector for a single point source is shown.

Csencsics, Wolf, and Schitter: Efficient framework for the simulation of translational and rotational laser . . .

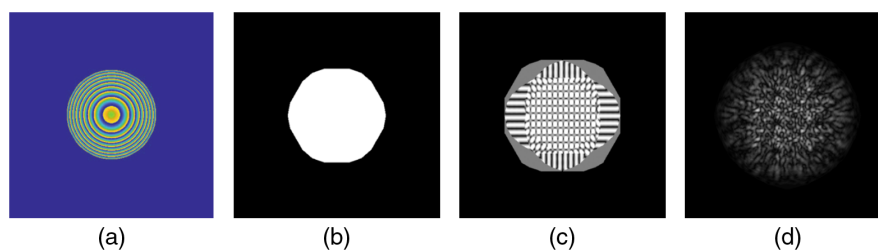


**Fig. 4** Simulated detector output for various numbers of point sources of an OLSP setup with additional 1 mm aperture. (a) The phase image on the detector with a single point source. (b) With a single point source no interference is obtained in the intensity image, (c) four point sources first constructive and destructive interference effects are observable. (d) 100 point sources lead to a fully developed speckle image.

The aperture and the detector are placed 39 and 78 mm away from the surface, respectively, with a detector size of  $4.2 \times 4.2$  mm and a pixel size of  $3 \times 3 \mu\text{m}$ . The distance between laser (wavelength of 632.8 nm) and surface is 50 mm and the angle  $\Theta$  is set to 35 deg. The number of point sources is varied from 1 over 4 to 100, using 1500 rays per point source for the subsequent ray tracing. Approximating the laser spot with a single point source leads to no interference effects on the detector. Increasing the number to 4 makes the effect of constructive and destructive interference visible but generates a nonsufficiently random pattern. The fringes for example represent regions where only two point sources interfere, while in the center region with the rectangular pattern all four point sources interfere. Setting the number of point sources to 100 leads to a good approximation of a fully developed speckle pattern for the given case, which is validated by correlation experiments with experimental data.

#### 4 Objective Laser Speckle Sensor Assemblies

To validate the results of the simulation framework as well as its capability to handle various system geometries, the output values for in- and out-of-plane target translations and rotations are compared against experimental measurements as well as analytic calculations. For this investigation, the four assemblies shown in Fig. 5 are used. The three simple OLSP assemblies Figs. 5(a)–5(c), with available analytic formulas for describing the speckle pattern shifts, are used to assess the capability to handle various system geometries, to obtain the sensitivities for in-plane translations and out-of-plane rotations, as well as to determine the susceptibility to crosstalk from other DoFs. The assembly with additional aperture (d), resembling the assembly of an integrated sensor capable of measuring in-plane translations or out-of-plane rotations together with out-of-plane translations at the same time,<sup>15</sup> is used to test the consideration of additional optical components and additional simulation outputs.

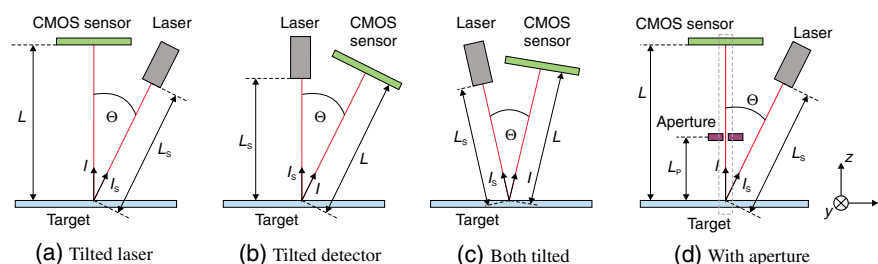


**Fig. 5** Configurations of experimental OLSP assemblies for verification of the simulation results. (a)–(c) Basic OLSP geometries for measuring translations or rotations and are composed of a laser, a detector, and the target itself. (d) The configuration of an integrated laser sensor with additional aperture for measuring in- and out-of-plane translations.

Csencsics, Wolf, and Schitter: Efficient framework for the simulation of translational and rotational laser...

The experimental setups are composed of a gray scale CMOS camera sensor (Type: DMK 22BUC03, Imaging Source GmbH, Bremen, Germany) as detector with  $744 \times 480$  pixels and a linear polarized HeNe laser (Model: 1108P, JDSU, Milpitas, California) with a wavelength of 632.8 nm, which is coupled into a single-mode fiber and directed toward the target, represented by a machined aluminium part with nonmodified surface. In-plane ( $x$  direction) and out-of-plane ( $z$  direction) target translations of the target are realized with two stacked position controlled linear stages (Type: VT-80 62309120, Physik Instrumente (PI) GmbH, Karlsruhe, Germany) with a resolution of 500 nm. Rotations ( $\Omega_x$ - and  $\Omega_z$ -directions) are enabled by position controlled rotation stages (ELL8K, Thorlabs Elliptec) with piezo resonant motors and internal encoders with a resolution of 0.0025 deg. Custom made mounting adapters are used to connect the individual rotational and linear stages to a motion system with serial kinematic. Further geometric parameters of the first three assemblies [(a)–(c)] include a laser distance to the target of 50 mm, a detector distance of 60 mm, and an angle  $\Theta$  of 35 deg. The image acquisition and processing is entirely done in MATLAB (MathWorks Inc., Natick, Massachusetts), which is used to implement functions that calculate the NCC peak shift for all four setups [(a)–(d)] as well as the CoG shift for the last setup (d). A correlation window size of  $64 \times 64$  pixel is used together with a twofold interpolation, which leads to an experimental resolution of  $\pm 1/4$  pixel (i.e.  $3 \mu\text{m}$ ).

#### 4.1 Translation Sensing

Considering the three basic OLSP assemblies for in-plane translation sensing and the relations for the motion of the speckle pattern on the detector Eqs. (1) and (2), first, rotations of the target need to be restricted to avoid crosstalk in the output  $A_\zeta$  and  $A_\eta$ , respectively. Second, it can be seen that for all three assemblies aligned in the  $xz$  plane,  $l_{S_y}$  and  $l_y$  become zero, resulting in the simplified unit vectors  $\vec{l} = (l_x, 0, l_z)^T$  and  $\vec{l}_S = (l_{S_x}, 0, l_{S_z})^T$  (see Fig. 1). With these two assumptions, the relations for speckle pattern displacement on the detector result to

$$A_\zeta = -a_x \left[ \frac{L_O}{L_S} (l_{S_x}^2 - 1) + l_x^2 - 1 \right] - a_z \left[ \frac{L_O}{L_S} l_{S_x} l_{S_z} + l_x l_z \right] = k_{x,t} \cdot a_x + k_{z,t} \cdot a_z, \quad (4)$$

$$A_\eta = a_y \left[ \frac{L_O}{L_S} + 1 \right] = k_{y,t} \cdot a_y, \quad (5)$$

with the target translations  $a_{x,y,z}$  and the translational sensitivities  $k_{x,t}$ ,  $k_{y,t}$ , and  $k_{z,t}$ . It is apparent that measuring translations in  $y$  direction is free of crosstalk, while the measurements of translations in  $x$  direction is also influenced by out-of-plane target motion. As long as  $k_{z,t}$  is significantly smaller than  $k_{x,t}$ , small out-of-plane translations are admissible and only slightly affecting the sensor output. Table 1 lists the calculated sensitivities for the three configurations. It clearly shows that the tilted laser assembly [see Fig. 5(a)] results in the highest value for  $k_{x,t}$  and the lowest value for  $k_{z,t}$  at the same time and is thus the most suitable one for sensing in-plane translations and the least susceptible one to out-of-plane crosstalk.

**Table 1** Sensitivities of basic OLSP assemblies to target translations.

	Tilted laser	Tilted detector	Both tilted
$k_{x,t}$ (mm/mm)	0.94	0.59	0.83
$k_{y,t}$ (mm/mm)	0.92	0.92	0.92
$k_{z,t}$ (mm/mm)	0.04	0.47	0.31

Csencsics, Wolf, and Schitter: Efficient framework for the simulation of translational and rotational laser...

**Table 2** Sensitivities of basic OLSP assemblies to target rotations.

	Tilted laser	Tilted detector	Both tilted
$k_{x,r}$ (mm/deg)	1.905	1.905	1.998
$k_{y,r}$ (mm/deg)	1.905	1.905	1.998
$k_{z,r}$ (mm/deg)	0.6	0.6	0.63

## 4.2 Rotation Sensing

A similar analysis can be conducted for the measurement of rotations of the target. Considering again the relations for the motion of the speckle pattern on the detector Eqs. (1) and (2), first, translations of the target need to be restricted to avoid crosstalk effects in the outputs. Second, the simplified unit vectors  $\vec{l} = (l_x, 0, l_z)^T$  and  $\vec{l}_S = (l_{Sx}, 0, l_{Sz})^T$  (see Fig. 1) are again applicable for the assemblies aligned in the  $xz$  plane. With these two assumptions, the relations for speckle pattern displacement on the detector result to

$$A_\zeta = \Omega_y [L_0(l_{Sz} + l_z)] = k_{y,r} \Omega_y, \quad (6)$$

$$A_\eta = \Omega_x [L_0(l_{Sz} + l_z)] + \Omega_z [L_0(l_{Sx} + l_x)] = k_{x,r} \Omega_x + k_{z,r} \Omega_z, \quad (7)$$

with the target rotations  $\Omega_{x,y,z}$  and the rotational sensitivities  $k_{x,r}$ ,  $k_{y,r}$ , and  $k_{z,r}$ . The measurement of rotations around the  $y$  axis is free of crosstalk, while the measurements of rotations around the  $x$  axis is also influenced by in-plane target rotations. Table 2 lists the calculated sensitivities for the three configurations. It shows that the sensitivities  $k_{x,r}$  and  $k_{y,r}$  for both rotational out-of-plane DoFs are equal for all three assemblies and that there is only marginal difference between the overall significantly higher susceptibility to crosstalk ( $k_{z,r}$ ), as compared to target translation. This means that all configurations are equally well suited for rotation sensing.

## 4.3 Combined Translation Sensing

To measure translations in all three DoFs with a single assembly and only minimal influence of the discussed crosstalk, the tilted laser assembly is extended by an additional aperture, as shown in Fig. 5(d), implementing an additional simple triangulation geometry. The setup is designed with slightly different geometric parameters for reasons of construction. The aperture is formed by an optical alignment target (SCPA1, Thorlabs Inc., Newton, New Jersey) with a diameter of 1 mm and is added between target and detector, entailing a not fully illuminated detector area. The geometric parameters are set to a laser distance of 50 mm, a detector distance of 75 mm, an aperture distance of 41 mm, and an angle  $\Theta$  of 39 deg. This configuration enables to distinguish between in- and out-of-plane translations of the target within a certain range of motion, as out-of-plane target translations transform into a CoG shift on the detector. The CoG shift due to out-of-plane translations has a significantly higher sensitivity than the effects on the speckle pattern itself, such that the out-of-plane component can be determined by the CoG shift.<sup>15</sup>

## 5 Experimental Results

To evaluate the accuracy and versatility of the simulation framework, experiments with the presented setups are conducted for (i) translation, (ii) rotation, and (iii) combined translation sensing. Performing subsequent quasi-static in- and out-of-plane target displacements and comparing simulation, measurement, and analytic results enables the evaluation of the simulation accuracy. For approximation of the laser spot, 100 point sources and 1500 rays per point source are used (see Sec. 3). For reasons of efficiency, the simulation is done for 10 displacements over an entire range of 200  $\mu\text{m}$  (translation) and 0.2 deg (rotation) and is linearly interpolated in-between, with the speckle pattern at 0  $\mu\text{m}$  serving as reference. With the used MATLAB implementation on a

Csencsics, Wolf, and Schitter: Efficient framework for the simulation of translational and rotational laser...

conventional personal computer, the simulation of a single displacement location takes about 90 s.

### 5.1 Translation Sensing

According to the analysis in Sec. 4.1, the assembly with the tilted laser in Fig. 5(a) results in the minimal crosstalk from out-of-plane translations to  $A_\zeta$ . Figure 6 shows the measured and simulated static decorrelation curves of this setup. The measurements show good agreement with the simulation and indicate that already a small spot shift of about  $100\ \mu\text{m}$  reduces the pattern correlation coefficient to below 50%, significantly reducing the signal-to-noise ratio.

The sensitivities of the setup with tilted laser calculate to  $k_{x,t} = 1 - L_O/L_S \cdot \cos^2(\Theta)$  and  $k_{z,t} = L_O/2L_S \cdot \sin(2\Theta)$ , showing the  $\Theta$ -dependency of both. In Fig. 7, the resulting simulated, measured, and analytically calculated NCC peak shifts are depicted as well as the simulation and measurement errors with respect to the analytically calculated, theoretical value. As expected, the sensitivity of the assembly for in-plane translations [see Fig. 7(a)] is about 1, while the crosstalk from out-of-plane translation on the speckle shift is as small as 4% for this setup [see Fig. 7(b)]. The error of the measurement shows steps with heights of less than  $3\ \mu\text{m}$ , which equals the resolution of the experimental setup (see Sec. 4). Due to slightly diverging slopes, the error increases toward larger translations but stays well below one pixel size. The error of the

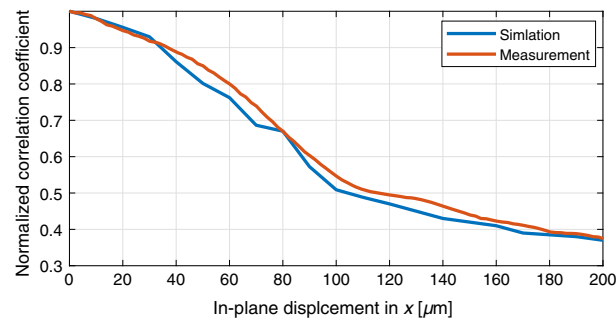


**Fig. 6** Speckle pattern decorrelation for in-plane target translation. Simulation and measurement result show good agreement and show that a shift of  $100\ \mu\text{m}$  reduces the pattern correlation coefficient to below 50%.

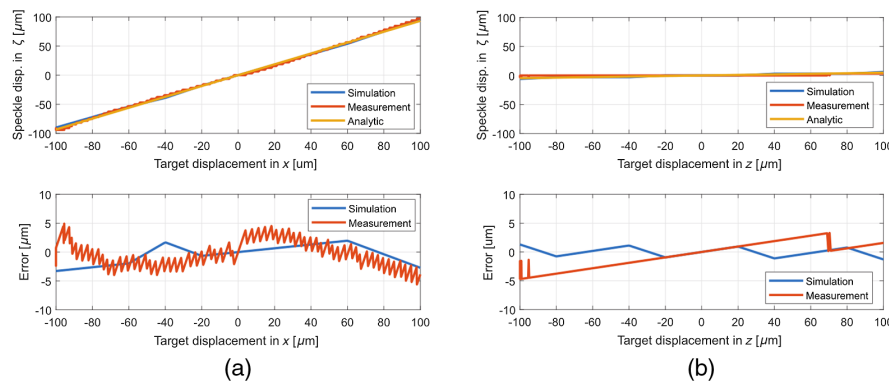


**Fig. 7** Target translation with tilted laser setup. Simulation output (blue), experimentally measured (red) and analytic results (yellow) of the speckle pattern shift on the detector. (a) The results for in-plane translations of the target and the related errors with respect to the analytic result. (b) The results for out-of-plane translations.

Csencsics, Wolf, and Schitter: Efficient framework for the simulation of translational and rotational laser . . .

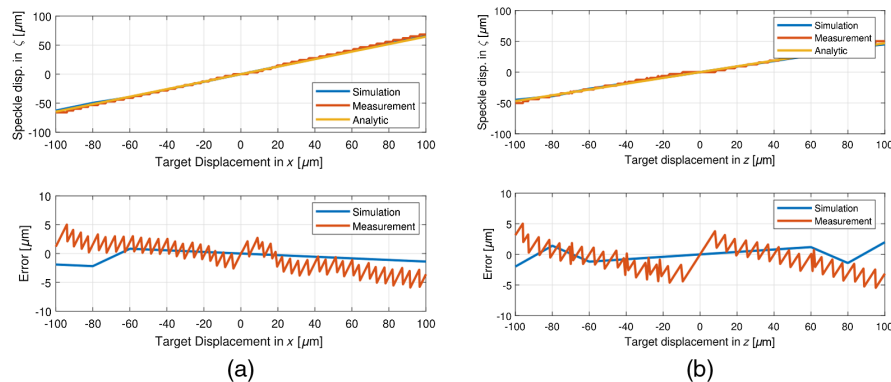


**Fig. 8** Target translation with tilted detector setup. Simulation output (blue), experimentally measured (red), and analytic results (yellow) of the speckle pattern shift on the detector. (a) The results for in-plane translations of the target and the related errors with respect to the analytic result. (b) The results for out-of-plane translations.

**Table 3** Simulation error of OLSP setup for in-plane (IP) and out-of-plane (OOP) translation of the target.

	Tilted laser		Tilted detector		Both tilted	
	IP	OOP	IP	OOP	IP	OOP
ptv error ( $\mu\text{m}$ )	5.2	2.6	3.0	3.9	4.4	5.1
rms error ( $\mu\text{m}$ )	1.9	0.9	1.2	1.2	1.4	1.1

in-plane simulation result shows a peak-to-valley (ptv) error of  $5.2 \mu\text{m}$  and a root-mean-square (rms) deviation of  $1.9 \mu\text{m}$ , giving a result even closer to the theoretical value than the measurement (error of  $11.1 \mu\text{m}$  ptv and  $2.5 \mu\text{m}$  rms). For out-of-plane translation, the obtained simulation result also matches the analytic result well, showing an error of  $0.9 \mu\text{m}$  rms.

The simulation and measurement results for the setup with tilted detector, which, according to the analysis, yields the lowest value for the sensitivity  $k_{x,t}$  and the highest value for the crosstalk sensitivity  $k_{z,t}$ , is depicted in Fig. 8. The simulation results in sensitivities of  $k_{x,t} = 0.60$  and  $k_{z,t} = 0.46$ , which show good matching with the analytically calculated respective values of  $0.59$  and  $0.47$ . As predicted, the sensitivity is only about 60% of the tilted laser assembly, while the crosstalk from out-of-plane translation additionally increases by a factor of more than 10. The assembly with tilted laser and detector shows a sensitivity which is about 80% of the first setup but also shows a crosstalk a factor 6 larger than the assembly with tilted laser (data not shown). Overall the simulation results for all three basic OLSP assemblies are in the same range of accuracy. The ptv and the rms errors with respect to the analytic result are for all setups listed in Table 3.

## 5.2 Rotation Sensing

Following the analysis in Sec. 4.2, all three basic OLSP assemblies result in a comparable sensitivity and crosstalk influence from in-plane rotations. The sensitivities calculate to  $k_{x,r} = k_{y,r} = L_O \cdot (1 + \cos(\Theta))$  and  $k_{z,r} = L_O \cdot \sin(\Theta)$ , respectively, again revealing the angle  $\Theta$  as the major design and tuning parameter. In Fig. 9, the resulting simulated, measured, and analytically calculated NCC peak shifts are depicted for the tilted laser configuration as well as the simulation and measurement errors with respect to the analytically calculated value. The simulated sensitivity of the assembly for out-of-plane rotation [see Fig. 9(a)] is about  $1.89 \text{ mm/deg}$  and

Csencsics, Wolf, and Schitter: Efficient framework for the simulation of translational and rotational laser...

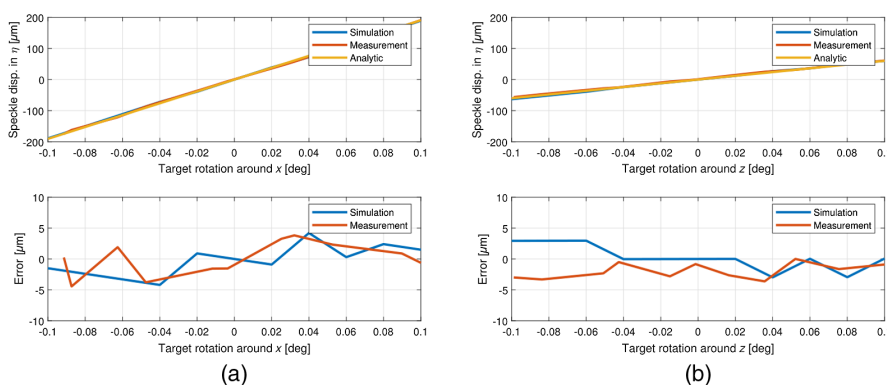


**Fig. 9** Target rotation with tilted laser setup. Simulation output (blue), experimentally measured (red), and analytic results (yellow) of the speckle pattern shift on the detector. (a) The results for out-of-plane rotations of the target and the related errors with respect to the analytic result. (b) The results for in-plane rotations.

**Table 4** Simulation error of OLSP setup for rotations of the target.

	Tilted laser		Tilted detector		Both tilted	
	IP	OOP	IP	OOP	IP	OOP
ptv error ( $\mu\text{m}$ )	6.0	8.4	4.2	6.9	5.0	7.8
rms error ( $\mu\text{m}$ )	2.0	2.4	1.5	2.0	1.9	2.3

matches the analytic value of 1.905 mm/deg well. The same holds for the crosstalk sensitivity to in-plane rotations [see Fig. 9(b)], which results to 0.62 mm/deg as compared with 0.6 mm/deg from the analytic calculation and equaling to significant 32% for this setup. The NCC peak shift error of the out-of-plane simulation result shows an error of 8.4  $\mu\text{m}$  ptv and 2.4  $\mu\text{m}$  rms, which is comparable to the variations of the experimental result. For in-plane rotations, the obtained simulation output also matches the analytic result well, showing an error of 2.0  $\mu\text{m}$  rms. The experiments reconfirm the simulation results, showing an rms error, which lies well below the 3  $\mu\text{m}$  resolution of the experimental setup. The simulation errors with respect to the analytic result are for all three basic OLSP assemblies listed in Table 4.

### 5.3 Combined Translation Sensing

For the integrated laser sensor with additional aperture enabling combined sensing of in- and out-of-plane translations [see Fig. 5(d)], the NCC peak shift is again evaluated as measure for in-plane translation and the CoG shift is used as additional simulation output to determine the out-of-plane translation of the target. For the analytic calculation of the CoG shift, geometric relations based on the nominal setup assembly are used. For calculation of the NCC peak shift, the aperture is neglected and Eq. (4) is used. The simulation is again evaluated for target displacements of 20  $\mu\text{m}$  steps over a motion range of 200  $\mu\text{m}$  and relative to the reference at 0  $\mu\text{m}$  displacement. To also demonstrate the relation between number of point sources and the achieved accuracy, the simulation is performed for 80 and 160 point sources. Figure 10 shows the simulated, measured, and analytically calculated values for both simulation outputs. The sensitivity to in-plane translations, the crosstalk, and the resulting simulation error is comparable to the basic OLSP configuration with tilted laser [see results without aperture in Fig. 7(a)], with the error being only insignificantly affected by the larger number of point sources. The resulting experimental sensitivity to out-of-plane translations due to the CoG shift is 0.67 and matches the analytic value well. With 80 point sources significant deviations of about 10  $\mu\text{m}$  between

Csencsics, Wolf, and Schitter: Efficient framework for the simulation of translational and rotational laser . . .

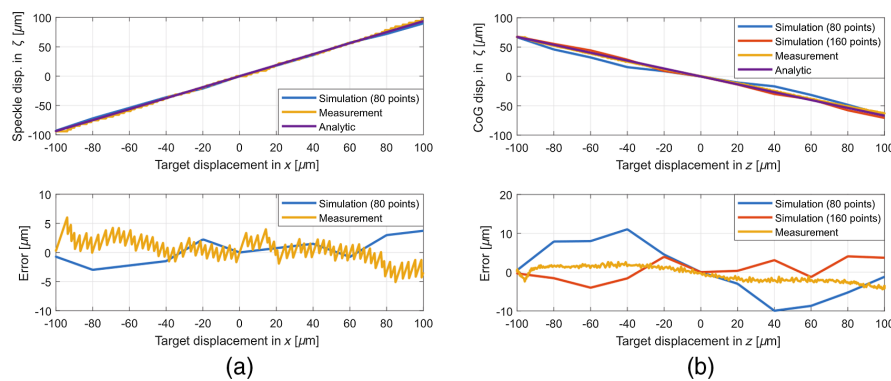


**Fig. 10** Simulation output for the integrated sensor setup with aperture. The result for 80 (blue) and 160 (red) point sources, the experimental data (yellow) and analytic results (violet) of (a) the speckle pattern shift for in-plane translations and (b) the CoG shift on the detector for out-of-plane translations are shown.

simulated and analytic value can be observed in Fig. 7(b) for out-of-plane translations around  $\pm 50 \mu\text{m}$ . Overall the simulation shows an error of  $20.9 \mu\text{m pTV}$  and  $6.6 \mu\text{m rms}$ . Increasing the number of point sources to 160, the accuracy is significantly improved and the error decreases to  $8.1 \mu\text{m pTV}$  and  $2.6 \mu\text{m rms}$ , which again even lies below the resolution of the experimental setup. The accuracy improvement, however, comes at the cost of a doubled computation time.

In summary, it is shown that the developed simulation framework enables an accurate simulation of speckle effects for target translations and rotations in various optical sensor assemblies including basic OLSP configurations as well as an integrated in- and out-of-plane sensor assembly with resulting simulation errors of less than  $2 \mu\text{m rms}$  and  $2.6 \mu\text{m rms}$  for for NCC peak and CoG shifts, respectively.

## 6 Conclusion

In this paper, an accurate, efficient, and versatile laser speckle simulation framework is developed for the design and analysis of laser-based optical sensor assemblies, which integrates the stochastic nature of laser speckle with the deterministic properties of ray-tracing simulations. It enables the calculation of several simulation outputs, such as correlation peak shift or CoG shift to determine the resulting sensitivity and crosstalk and identify the best performing system configuration for a given requirement and measurement principle. The simulation framework is capable of considering the entire system geometry including the locations, orientation, and size of the laser source, the target surface, the detector (with number and size of pixels), and apertures, mirrors or lenses, if applicable. The laser spot on the target is approximated by a sufficiently large number of individual point sources with random height distribution in the range of the surface roughness, where each point source is then simulated by  $N_2$  rays that are traced through the optical system and provide the respective intensity and phase at each detector pixel. The speckle image on the detector is calculated by complex summation of the intensity and phase image matrix of all point sources on the detector. To validate the simulation results for various system geometries, they are compared against the experimental data and analytical results of four designed laser-speckle-based sensor setups for measuring in- and out-of-plane translation and rotation of a target. The accuracy of the simulation framework for target translation and rotation is demonstrated by resulting simulation errors of the NCC peak shift on the detector of less than  $2 \mu\text{m rms}$  and  $2.4 \mu\text{m rms}$ , respectively, which lie well below the resolution of the designed sensor assemblies. For the combined translational displacement sensor, the additionally simulated CoG shift due to out-of-plane translations resulted in an error as small as  $2.6 \mu\text{m rms}$ . Increasing the number of point sources is shown to reduce the error of the CoG shift output, while not significantly affecting the NCC peak shift output, such that an individual tradeoff

Csencsics, Wolf, and Schitter: Efficient framework for the simulation of translational and rotational laser...

between computation time and accuracy is required for each sensor system design. Future work includes the advancement of the simulation tool in terms of computational efficiency and the application for uncertainty estimations of laser-based sensor systems.

## References

1. D. Wertjanz, E. Csencsics, and G. Schitter, "3 DoF vibration compensation platform for robot-based precision inline measurements on free-form surfaces," *IEEE Trans. Ind. Electron.* **69**(1), 613–621 (2022).
2. Y. Chen and F. Dong, "Robot machining: recent development and future research issues," *Int. J. Adv. Manuf. Technol.* **66**(9-12), 1489–1497 (2013).
3. M. Ries et al., "Real-time 3D target tracking in MRI guided focused ultrasound ablations in moving tissues," *Magn. Reson. Med.* **64**(6), 1704–1712 (2010).
4. A. Krupa, G. Fichtinger, and G. D. Hager, "Full motion tracking in ultrasound using image speckle information and visual servoing," in *Proc. IEEE Int. Conf. Rob. and Autom.*, pp. 2458–2464 (2007).
5. D. Imkamp, R. Schmitt, and J. Berthold, "Blick in die zukunft der fertigungsmesstechnik - die vdi/vde-gma roadmap fertigungsmesstechnik 2020," *Tech. Mess.* **79**(10), 433–439 (2012).
6. M. Thier et al., "Six degree of freedom vibration isolation platform for in-line nanometrology," *IFAC-PapersOnLine* **49**(21), 149–156 (2016).
7. C. P. Keferstein and W. Dutschke, *Fertigungsmesstechnik*, Springer Vieweg, Wiesbaden (2010).
8. P. Rastogi and D. Inaudi, *Trends in Optical Non-Destructive Testing*, Elsevier Science, Kidlington, Oxford, England (2000).
9. S. Schneider, Y. Gautam, and B. Zagar, "Application of a locally operating laser-speckle strain sensor," *IEEE Trans. Instrum. Meas.* **52**(4), 1025–1029 (2003).
10. I. Yamaguchi, T. Takemori, and K. Kobayashi, "Stabilized and accelerated speckle strain gauge," *Opt. Eng.* **32**(3), 618–625 (1993).
11. T. O. Charrett, T. Kissinger, and R. P. Tatam, "Workpiece positioning sensor (WPOS): a three-degree-of-freedom relative end-effector positioning sensor for robotic manufacturing," *Procedia CIRP* **79**, 620–625 (2019).
12. R. Paris, M. Melik-Merkumians, and G. Schitter, "Probabilistic absolute position sensor based on objective laser speckles," *IEEE Trans. Instrum. Meas.* **65**(5), 1188–1196 (2016).
13. R. Paris, T. Thurner, and G. Schitter, "Compensation based displacement measurement using objective laser speckles," *IFAC Proc. Volumes* **46**(5), 264–270 (2013).
14. T. O. Charrett et al., "A non-contact laser speckle sensor for the measurement of robotic tool speed," *Rob. Comput. Integr. Manuf.* **53**, 187–196 (2018).
15. E. Csencsics, "Integrated compensation-based laser sensor system for in-plane and out-of-plane target tracking," *Appl. Opt.* **59**(20), 6138–6147 (2020).
16. R. G. Dorsch, G. Häusler, and J. M. Herrmann, "Laser triangulation: fundamental uncertainty in distance measurement," *Appl. Opt.* **33**(7), 1306–1314 (1994).
17. D. D. Duncan and S. J. Kirkpatrick, "The copula: a tool for simulating speckle dynamics," *J. Opt. Soc. Am. A* **25**(1), 231–237 (2008).
18. D. D. Duncan and S. J. Kirkpatrick, "Algorithms for simulation of speckle (laser and otherwise)," *Proc. SPIE* **6855**, 685505 (2008).
19. A. Federico et al., "Simulation of dynamic speckle sequences and its application to the analysis of transient processes," *Opt. Commun.* **260**(2), 493–499 (2006).
20. I. Yamaguchi, "Digital simulation of speckle patterns," *Proc. SPIE* **10834**, 1083409 (2018).
21. D. J. Burrell et al., "Wave-optics simulation of dynamic speckle: II. In an image plane," *Appl. Opt.* **60**(25), G77–G90 (2021).
22. E. Csencsics, T. Wolf, and G. Schitter, "Speckle simulation tool for the design of laser-based displacement sensors," *Proc. SPIE* **11782**, 117820G (2021).
23. J. W. Goodman, "Some fundamental properties of speckle," *J. Opt. Soc. Am.* **66**(11), 1145–1150 (1976).

Csencsics, Wolf, and Schitter: Efficient framework for the simulation of translational and rotational laser...

24. I. Yamaguchi, "Speckle displacement and decorrelation in the diffraction and image fields for small object deformation," *Opt. Acta* **28**(10), 1359–1376 (1981).
25. M. Sjoedahl, "Calculation of speckle displacement, decorrelation, and object-point location in imaging systems," *Appl. Opt.* **34**(34), 7998–8010 (1995).
26. M. Sjoedahl, "Accuracy in electronic speckle photography," *Appl. Opt.* **36**(13), 2875–2885 (1997).
27. Y. Petrov, "Optometrika—MATLAB library," 2021, <https://de.mathworks.com/matlabcentral/fileexchange/45355-optometrika>.

**Ernst Csencsics** is an assistant professor for measurement systems in the Advanced Mechatronic Systems group at the Automation and Control Institute (ACIN) of TU Wien. He received his MSc and PhD degrees (sub auspiciis) in electrical engineering from TU Vienna, Austria, in 2014 and 2017, respectively. His primary research interests are on high-performance mechatronic systems, holistic methods for multidisciplinary system design and integration, optomechatronic measurement and imaging systems, precision engineering, and robot-based in-line metrology.

**Tobias Wolf** is a master's student in energy systems and automation technology at TU Wien. He conducted his bachelor's thesis at the ACIN and received his BSc degree in electrical engineering from TU Wien in 2018. Since then he has been working as a student researcher at ACIN, focusing on the development speckle-based measurement systems and related simulation tools.

**Georg Schitter** is a professor for advanced mechatronic systems at the ACIN of TU Wien. He received his MSc degree in electrical engineering from TU Graz, Austria, in 2000, and his MSc and PhD degrees in nanotechnology from ETH Zurich, Switzerland, in 2004. His research focuses on mechatronic systems for applications in the high-tech industry, scientific instrumentation, and mechatronic imaging systems, such as AFM and LIDAR systems, telescope systems, adaptive optics, and lithography systems.